Study of the design and mechanical performance of a GFRP-concrete composite deck

Yong Yang [a], Yicong Xue [*], Yunlong Yu [c], Ruyue Liu [d] and Shoufeng Ke [e]

School of Civil Engineering, Xi'an University of Architecture & Technology, Xi'an, Shaanxi 710055, China

Abstract. A GFRP-concrete composite bridge deck is presented in this paper. This composite deck is composed of concrete and a GFRP plate and is connected by GFRP perfobond (PBL) shear connectors with penetrating GFRP rebar. There are many outstanding advantages in mechanical behavior, corrosion resistance and durability of this composite deck over conventional reinforced concrete decks. To analyze the shear and flexural performance of this GFRP-concrete composite deck, a static loading experiment was carried out on seven specimens. The failure modes, strain development and ultimate bearing capacity were thoroughly examined. Based on elastic theory and strain-based theory, calculation methods for shear and flexural capacity were put forward and revised. The comparison of tested and theoretical capacity results showed that the proposed methods could effectively predict both the flexural and shear capacity of this composite deck. The ACI 440 methods were relatively conservative in predicting flexural capacity and excessively conservative in predicting shear capacity of this composite deck. The analysis of mechanical behavior and the design method can be used for the design of this composite deck and provides a significant foundation for further research.

Keywords: GFRP-concrete composite deck; flexural performance; shear performance; design method; experimental study

1. Introduction

In recent years, advanced composite materials have been widely used in the civil engineering field, due to their favorable characteristics such as being light weight and having high strength and excellent resistance to corrosion. A good example is glass fiber-reinforced polymer (GFRP) material, which is being used more and more widely in structures that require high durability, such as coastal bridges. Compared with traditional materials, such as concrete and steel, GFRP is lightweight and less vulnerable to harsh or extreme environments. Most bridges, as part of the critical infrastructure in cities, are exposed to an aggressive atmosphere, and when they are structurally damaged or functionally obsolete, there may be large costs associated with their maintenance or retrofitting. It is necessary to develop innovative structural elements that can resist corrosion and enhance the durability of bridge systems. GFRP bridges have been an advisable solution to such problems for a long time, but due to their high cost, the use of GFRP for whole bridges has been limited. In addition, GFRP—similar to steel—always buckles when subjected to a compressive force; therefore, it is very complicated to understand well and calculate accurately.

With the aim of addressing the deficiencies in the corrosion behavior and durability of traditional bridges, as well as taking full advantage of advanced materials, some

researchers have examined the benefits of combining concrete and GFRP materials. Mirmiran *et al.* (2001) believed that the combination of GFRP material and concrete was an effective composite form in GFRP composite members. In their structural systems, concrete was located in the compressive zone to provide stability and flexural rigidity to the composite members, with the GFRP plate at the tension zone, where it served as longitudinal reinforcement. In this design, the local buckling of the GFRP plates can be avoided, and no other reinforcement is needed. After recognizing the advantages of GFRP-concrete composite members, some experimental research has been conducted on the behavior of GFRP-concrete composite decks. Cho *et al* proposed a GFRP concrete composite deck using concrete wedge and coarse sand coating, and Sarir *et al* performed numerical simulation based on the Cho's test results (Sarir *et al.* 2016, Cho *et al.* 2010). Xin *et al.* (2015) investigated the fatigue and thermal performance of a hybrid GFRP-concrete bridge deck. Zhu and Lopez presented a lightweight GFRP composite bridge deck, constituted by pultruded tube and grouted panel, and performed flexure tests (Zhu and Lopez 2014). He *et al* performed static test of a movable hybrid GFRP and concrete bridge deck with box GFRP girder and T-upstands (He *et al.* 2012). Pantelides *et al* conducted a series static loading tests of lightweight concrete precast deck panels reinforced with GFRP bars (Pantelides *et al.* 2012). Neto and Rovere proposed a composite concrete-GFRP slab with I-shape GFRP profiles and concrete (Neto and La Rovere 2010). Keller *et al.* (2007) proposed a hybrid sandwich bridge deck, consisted of a GFRP plate with T-upstands, a

---

*Corresponding author, Ph.D. Candidate,
E-mail: xjdxyc@foxmail.com

core made of lightweight concrete and a compressive skin made of ordinary concrete. Hanus *et al* presented a bridge deck reinforced with a structural FRP stay-in-place form (Hanus *et al*. 2009).

The reviewed research shows a high potential for GFRP-concrete composite construction where each material optimally used. Although there has been some research on GFRP-concrete composite decks, many problems remain, such as optimizing the composite form and finding effective ways to connect the GFRP plate to the concrete. Moreover, few approaches focus on the complete mechanical behavior including flexural performance and shear performance with the increasing of the shear span. This paper proposed a new GFRP-concrete composite deck that should propel the development of GFRP-concrete composite deck and prevent some of aforementioned problems, which is illustrated in Fig. 1. The pultruded GFRP plate with perfobond strip connectors made of GFRP (PBL connectors) can serve as a permanent formwork for concrete and provide tensile resistance, so no other temporary formwork and reinforcement are needed. The concrete is fully bonded to the GFRP plate by means of the PBL shear connectors, which are not only employed to develop the shear stress transfer on the interface between the two different materials but also to enhance the flexural rigidity during the construction stage. Meanwhile, the sand coating was applied on the top surface of both the GFRP plate and the PBL connectors to further enhance the bonding performance. There is no steel rebar in this composite deck, so corrosion will be avoided, which makes it particularly suitable for marine structures.

To investigate the mechanical behavior of this composite deck, an experiment with seven specimens was carried out. In this paper, the effect of shear span-to-depth ratio and typical failure modes are critically examined. Based on the experimental observations and test results, corresponding design methods are put forward later in this paper.

2. Test program

2.1 Specimen design

Seven GFRP-concrete composite deck specimens were designed and constructed according to General Code for Design of Highway Bridges and Culverts (JTG D60 2015). The main experimental parameter was the shear span length. The shear span aspect ratio, defined as the shear span length divided by the total height of the composite deck, varied from 2.0 to 7.0 to investigate the complete mechanical behaviors with the change of shear span. Fig. 2 shows the main details of the PBL connector.

The sizes of cross section, materials used and the number of PBL connectors in each of the specimens were nominally identical. The specimen was composed of three parts, namely the GFRP plate, cast-in-place concrete and PBL connectors. The PBL connectors consisted of perforated ⊥ shape GFRP elements bonded onto the pultruded GFRP plate by epoxy resin and a number of penetrating GFRP rebar. The prefabricated holes (20 mm diameter) and penetrating GFRP rebar (8 mm diameter) enhanced the shear stress transfer due to the concrete dowel. The sand coating applied on the top surface of both the GFRP plate and the PBL connectors. Once the concrete had cured, the three components were joined together and behaved structurally as an integral member. The construction process is illustrated in Fig. 3 and the parameters of the specimens are summarized in Table 1.

2.2 Material properties

The GFRP material, matrix resin and pultrusion technique of the GFRP plate were designed per the requirements, a woven fabric made of E-glass fiber was determined as GFRP reinforcement. Vinyl ester resin was chosen as the matrix. The pultruded profiles, the main part
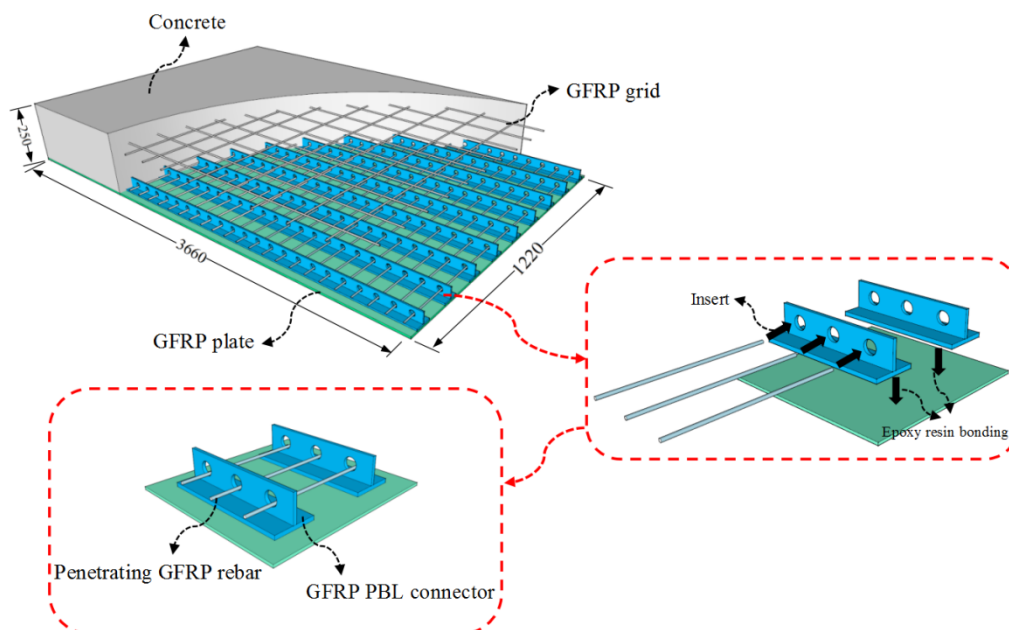

Fig. 1 Diagram of the composite deck (unit: mm)

(a) Cross section of the specimens
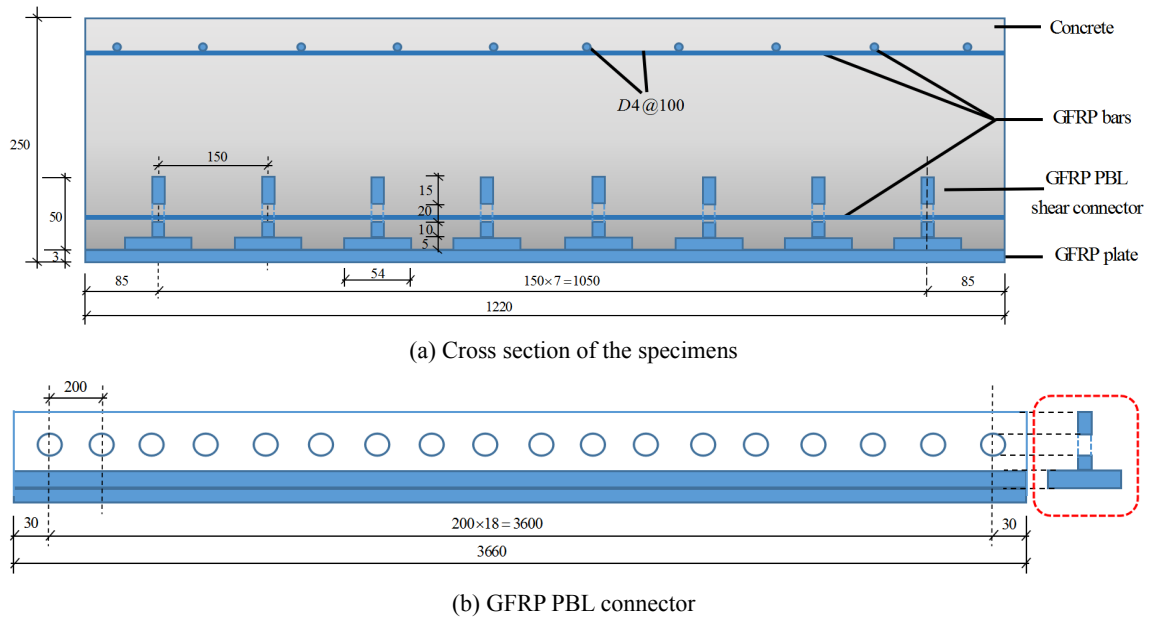

(b) GFRP PBL connector

Fig. 2 Details of the specimens (unit: mm)

(a) Sand coating   (b) Reinforcing and penetrating rebar fasten

Fig. 3 Fabrication process of the specimens

Table 1 Details of specimens

ID	Span length l_0/mm	Height h/mm	Width b/mm	Shear span a/mm	Shear span aspect ratio λ	PBL shear connector
FC1	3510	250	1220	500	2.0	5×50×3660@200
FC2	3510	250	1220	800	3.2	5×50×3660@200
FC3	3510	250	1220	1000	4.0	5×50×3660@200
FC4	3510	250	1220	1125	4.5	5×50×3660@200
FC5	3510	250	1220	1500	6.0	5×50×3660@200
FC6	3510	250	1220	1550	6.2	5×50×3660@200
FC7	3510	250	1220	1730	7.0	5×50×3660@200

*Note: The dimensions of PBL connector are expressed as thickness×height×length@the longitudinal spacing of holes

of the GFRP plate and PBL shear connectors, were composed of fiber glass rovings embedded in a matrix, with a fiber volume of 55%, and of laminates made of continuous strand mats. Other detailed properties of GFRP material provided by manufacturer are listed in Table 2, and the rule of mixtures (Kaw 2006) is applied here to obtain the calculated mechanical properties of each individual laminae. Meanwhile, tensile tests were conducted according

to Fiber-reinforced plastics composites - Determination of tensile properties (GB/T 1447 2005), and the measured GFRP strengths shown in Table 3 were determined based on the tensile tests of samples taken from the GFRP plate, PBL connectors and GFRP rebar.

The concrete strength was determined based on compression tests of concrete cubes, which were conducted according to the Chinese standards (GB 50010-2010). The

Table 2 Properties provided by manufacturer and predicted based on micro-mechanics model

	Category	E_1 /GPa	E_2 /GPa	G_{12} /GPa	v_{12} /GPa
Material	E-Glass fiber	71.8	-	26.9	0.21
	Vinyl ester resin	3.9	-	1.4	0.32
Predicted laminae property	Continuous strand mat	7.1	7.1	1.9	0.37
	Glass rovings /Vinyl ester resin	41.2	8.1	2.9	0.26

*Note: The subscript 1 is the longitudinal direction of the profile; the subscript 2 is the transverse direction of the profile

Table 3 Measured material properties of GFRP

Material	Element	GFRP material	E_f/GPa	f_u/MPa
GFRP	PBL connector	E-Glass fiber/vinyl ester resin	25.1	457
	plate	E-Glass fiber/vinyl ester resin	25.1	443
	rebar	E-Glass fiber/vinyl ester resin	27.0	510

*Note: The subscript 1 is the longitudinal direction of the profile; the subscript 2 is the transverse direction of the profile

(a) Schematic diagram of four-point test

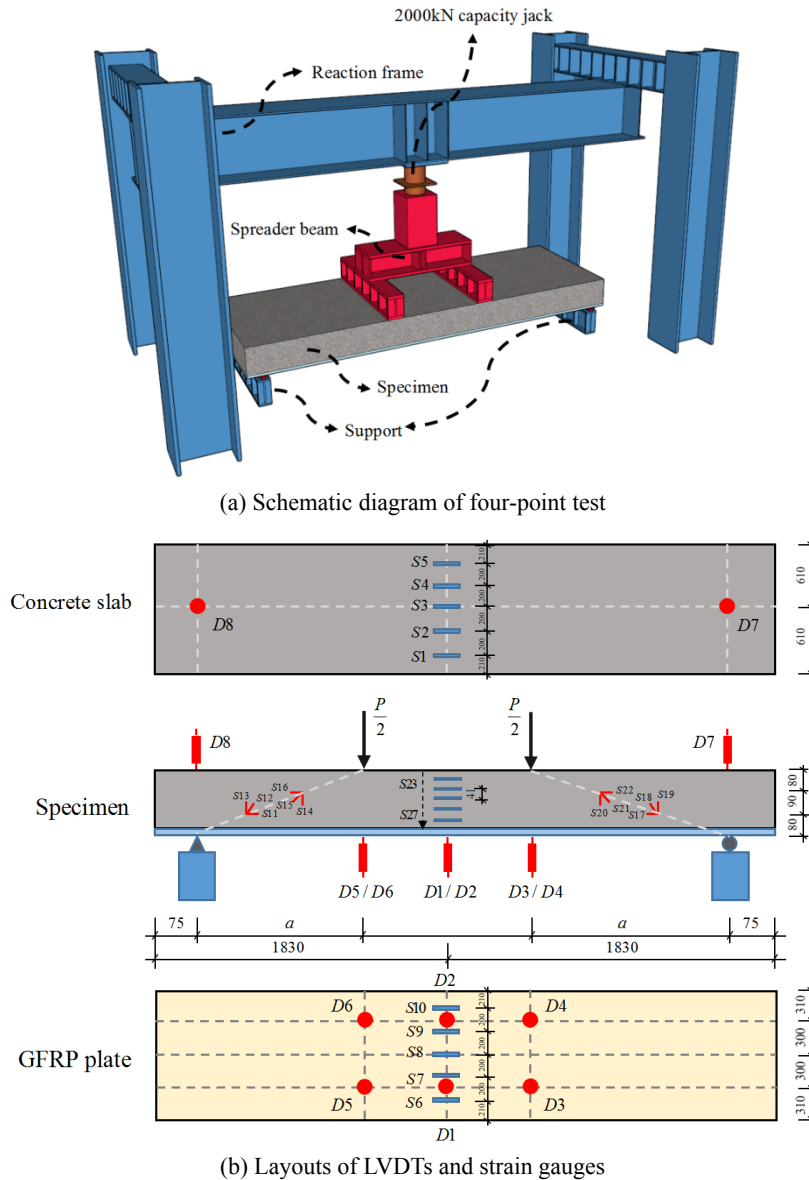(b) Layouts of LVDTs and strain gauges

Fig. 4 Loading device and layouts of strain gauges and LVDTs

axial compressive strength of the concrete was calculated to be 0.8 times as the cubic strength. The mean value of the measured cubic compressive strength and Young's modulus were 54.2 MPa and 29.0 GPa.

2.3 Test setup

The experiment was conducted in the *Structural Engineering Key Laboratory at Xi'an University of Architecture and Technology*. A four-point test procedure was adopted and a 2000 kN hydraulic jack was used to apply monotonic load. In the test, the load was applied to the top of the concrete via a spreader beam and two support beams. The test apparatus generated two shear spans near the ends and a pure bending span in the middle of the simply supported deck. The length of the shear span varied in different specimens with different shear demands. During the test process, all of the deflections of the specimens at the central point, loading point and two supports were measured using linear variable differential transformers (LVDTs). When the shear span aspect ratio was greater than 5.0, a set of strain gauges were set vertically along the height of the cross section at the mid-span to verify the plane section hypothesis. The tensile strain of the GFRP plate as well as the compressive strain of the concrete was also critically examined. When the shear span aspect ratio was less than 5.0, strain rosettes were set up in the shear span. The loading device and layouts of strain gauges and LVDTs are shown in Fig. 4.

3. Experimental results

3.1 Experimental phenomena and failure modes

For specimen FC 1-FC 4, the crack initiated at the mid-span at about $0.1P_u$. The following flexural cracks appeared with the load increasing but the crack propagations were constrained. Diagonal shear cracks were observed at approximately 0.4-$0.8P_u$, and these cracks stretched as the load increased. Flexural cracks that formed due to pure

bending at the mid-span propagated slowly and the final failure mode was dominated by the diagonal shear crack extending through the entire height of the critical section.

For specimen FC 5-FC 7, flexural cracks developed prior to shear cracks, the first bending crack appeared at about $0.1P_u$. Then the initial crack propagated and new flexural cracks were observed with increasing of the load. The first bending-shear cracks did not appear until the specimen was loaded to approximately $0.6P_u$. These specimens suffered slight concrete crushing and layer laceration of the GFRP plate when failure occurred.

Therefore, the final failure modes of the specimens were mainly dependent on the shear span aspect ratio.

For all specimens, no obvious longitudinal cracks indicating slippage were observed on the interface, which showed that the PBL connectors transferred the longitudinal shear stress well and the specimens behaved fully composite. Photos of the crack patterns and the final failure modes of the specimens are shown in Fig. 5.

4. Analysis of experimental results

4.1 Load deflection response

The load-deflection curves at the mid-span of the specimens are traced in Fig. 6. The ultimate loads are summarized in Tables 4 and 5 along with the calculated capacity. The results clearly indicate that the shear span aspect ratio has the most significant influence on the behavior of this composite deck. With increasing shear span, the deformability of the specimens decreases remarkably. The figures show that a lower shear span aspect ratio correlates with higher ultimate capacity at the expense of deformability. Because of the inherent brittlement of GFRP material, which means that there is no obvious yield point, specimens suffered brittle failure without obvious warning signs. On the other hand, as a benefit of the pultrusion technique, layer laceration of the GFRP plate was found to be accompanied by some clear noise when the specimen was approaching its limit, which could be

(a) FC 1   (b) FC 2   (c) FC 4

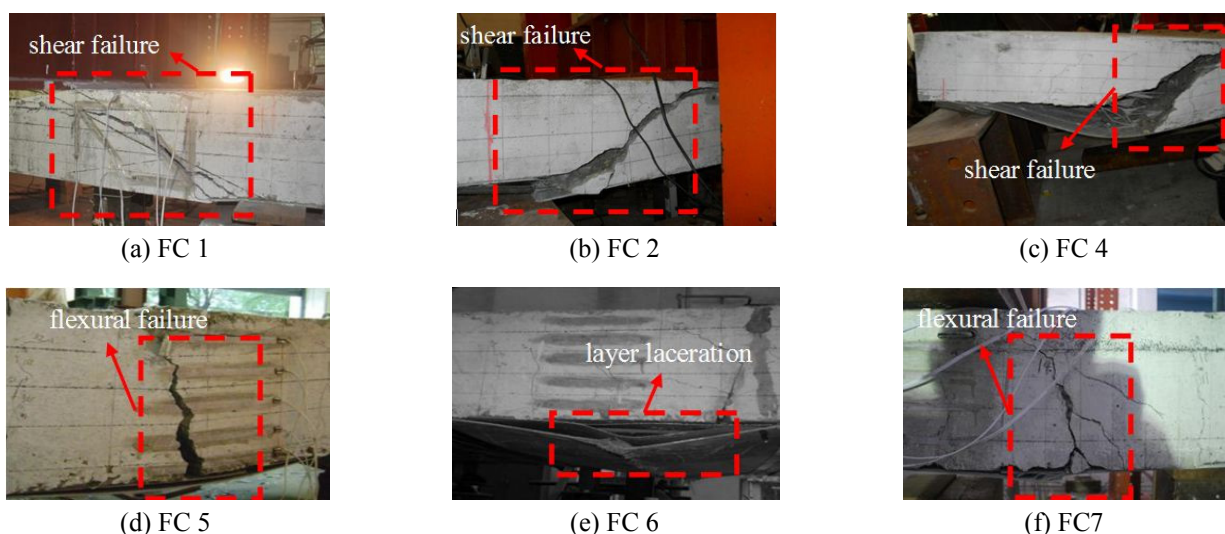(d) FC 5   (e) FC 6   (f) FC7

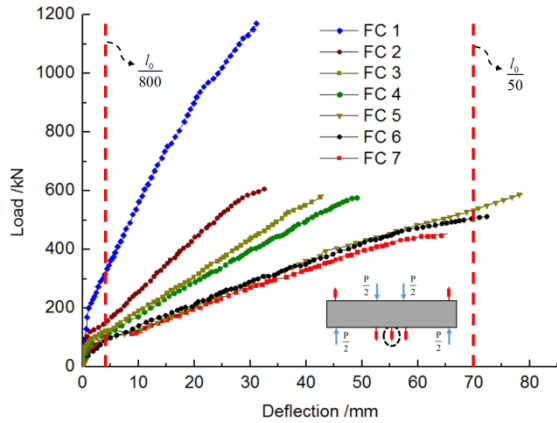Fig. 5 Typical failure patterns: (a)-(c) shear failure and (d)-(f) flexural failure
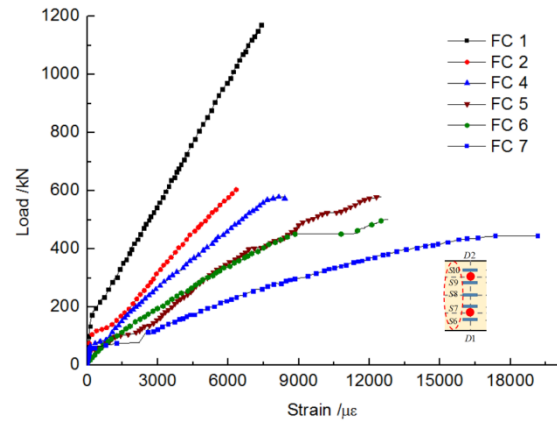
Fig. 6 Load vs. deflection curves at the mid-span

Fig. 7 Load-strain relationship of GFRP plate

Table 4 Major test results for specimens failed in flexure

ID	P_u/kN	M_u/kN·m	Δ_u/mm	Failure mode	M_{c-T}/kN·m	M_u/M_{c-T}	M_{c-ACI}/kN·m	M_u/M_{c-ACI}
FC 5	590	443	78.9	Flexure	443	1.00	300	1.48
FC 6	511	396	72.7	Flexure	443	0.89	300	1.28
FC 7	455	398	66.4	Flexure	443	0.90	300	1.33
Average ratio of measured to calculated value						0.93		1.36
Coefficient of variation						0.05		0.06

*Note: P_u is the peak load, M_u is the tested flexural capacity, Δ_u is the ultimate deflection, M_{c-T} is the flexural capacity obtained by theoretical method, M_{c-ACI} is the flexural capacity obtained by ACI 440 method

Table 5 Major test results for specimens failed in shear

ID	P_u/kN	V_u/kN	Δ_u/mm	Failure mode	V_{c-T}/kN	V_u/V_{c-T}	V_{c-S}/kN	V_u/V_{c-S}	V_u/V_{c-ACI}
FC 1	1165	583	31.2	Shear	421	1.38	505	1.15	5.45
FC 2	608	304	32.7	Shear	324	0.94	361	0.84	2.84
FC 3	594	297	49.5	Shear	309	0.96	303	0.98	2.77
FC 4	577	289	51.4	Shear	304	0.95	276	1.05	2.70
Average ratio of measured to calculated value						1.06		1.01	3.44
Coefficient of variation						0.18		0.11	0.34

*Note: P_u is the peak load, V_u is the tested shear capacity, Δ_u is the ultimate deflection, V_{c-T} is the shear capacity obtained by theoretical method, V_{c-S} is the shear capacity obtained by simplified method, V_{c-ACI} is the shear capacity obtained by ACI 440 method

regarded as an early warning of failure. As shown in Fig. 6, the mid-span deflections of specimens far exceeded the allowable deflection at service load in AASHTO, $l_0/800$, and those of specimens failed in flexure almost reached $l_0/50$.

4.2 Typical load strain curve

A considerable number of electrical-resistance strain gauges were arranged at the mid-span of the GFRP plate and top surface of the concrete to monitor the strain responses. The typical load-strain curves at the mid-span are summarized in Fig. 7. For the GFRP plate, the figure clearly indicates that the strain developed linearly during the test process and the ultimate strain approached approxi-

mately 8000 $\mu\varepsilon$-16000 $\mu\varepsilon$. Meanwhile, quasi-yield platforms are observed in the specimens that suffered flexural failure due to the split-tear phenomenon of pultruded GFRP materials, which meant that the GFRP plate had performed well. As for the concrete, slight crushing was observed near the maximum load in most specimens.

For specimens FC 5-FC 7 which failed in flexure, as a conventional procedure, a set of strain gauges was arranged along the entire height of the section to verify the section assumption. As shown in Fig. 8, the result agrees with the theory, in which strain is linearly distributed along the height of the section throughout the experiment. Therefore, Bernoulli's hypothesis of plane-strain distribution is valid in this composite deck.
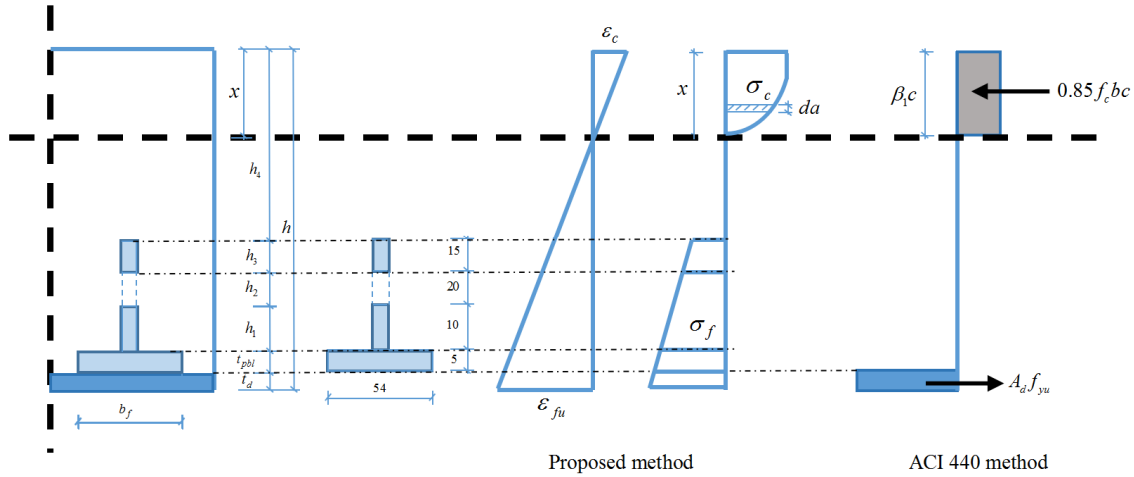
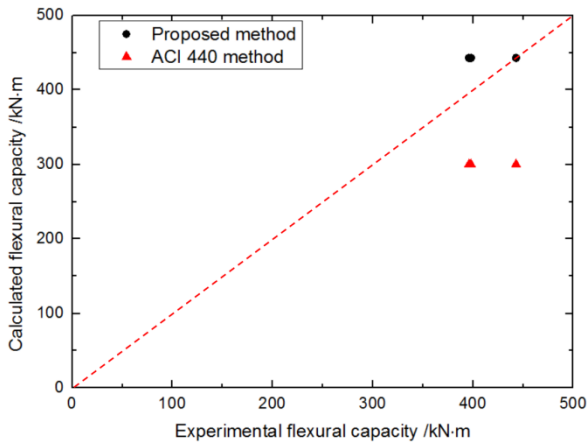Fig. 9 Calculation sketch for flexural capacity

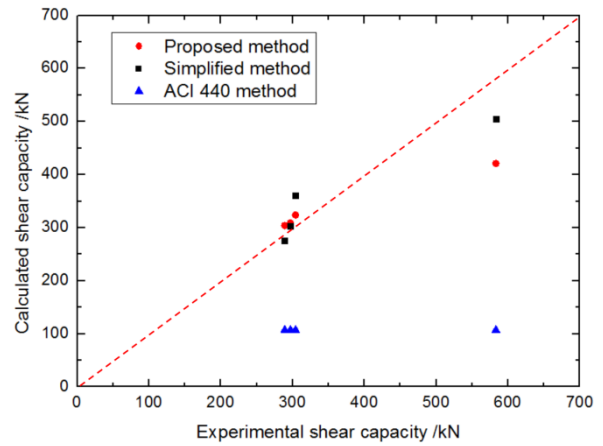Fig. 10 Comparison of calculated and experimental flexural capacity

Fig. 11 Comparison of calculated and experimental shear capacity

5. Analysis of flexural capacity

5.1 Basic assumptions

In the test, no obvious slippage was observed on the interface between the GFRP plate and concrete, which indicated that the specimens were sufficiently composite. As GFRP material is generally assumed to be linearly elastic materials, and the composite decks have been proven to be fully connected during the experiment, the theory of elasticity is applied here to analyze the flexural capacity. The assumptions made in analyzing these tests can be summarized as follows:

(1) The plane-section assumption was satisfied.
(2) The tensile strength of the concrete was relatively small and therefore neglected.
(3) For simplicity, the Rüsch constitutive law was adopted to describe the behavior of concrete subjected to compression.
(4) The ultimate strain of the GFRP plate was limited to 12000 $\mu\varepsilon$. The peak strain and ultimate strain of concrete were 0.002 and 0.003, respectively.
(5) The height of the PBL connectors is relatively small compared to the total height of the composite deck, so the natural axis can be regarded as passing through the concrete.

The calculation sketch is presented in Fig. 9.

5.2 Design procedure

For the composite decks under flexure, the flexural capacity varies with the strain of the top concrete. To simplify the design procedure, two different cases were defined.

(1) Case 1: $\varepsilon_c \leq \varepsilon_0$, $x \leq h_4$ and $x \leq \dfrac{\varepsilon_{cu}}{\varepsilon_{cu} + \varepsilon_{fu}}$

For the concrete and the GFRP plate, the stress can be obtained as follows

$$\sigma_c = f_c \frac{\varepsilon_c}{\varepsilon_0} (2 - \frac{\varepsilon_c}{\varepsilon_0}) \tag{1}$$

$$\sigma_f = E_f \varepsilon_f \tag{2}$$

The resultant point of the concrete can be determined as

$$C = \int_0^x \sigma_c b da = \int_0^x f_c \left[2\frac{\varepsilon_c}{\varepsilon_0} - \left(\frac{\varepsilon_c}{\varepsilon_0}\right)^2 \right] b da = \frac{6 f_c b x^2 (h - 3x)}{(h - x)^2} \quad (3)$$

The depth of the compression zone can be calculated using the equilibrium condition

$$\frac{6 f_c b x^2 (h - 3x)}{(h - x)^2} = \frac{E_f \varepsilon_{fu}}{h - x} [A_d (h - x - t_d)$$
$$+ A_{pbl1} (h - x - t_d - t_{pbl})$$
$$+ A_{pbl2} (h - x - t_d - t_{pbl} - h_1) \quad (4)$$
$$+ A_{pbl3} (h_4 - x)]$$

Note that the distance from the natural axis to the resultant point of the concrete is determined as

$$x_c = \frac{1}{C} \int_0^x \sigma_c b a da = x \left[\frac{4h - 13x}{6(h - 3x)} \right] \quad (5)$$

Finally, the flexural capacity of this composite deck can be calculated from Eq. (6)

$$M_u = \frac{6 f_c b x^2}{h - x} \left(1 - \frac{2x}{h - x} \right) x_c$$
$$+ \frac{E_f \varepsilon_{fu}}{h - x} [A_d (h - x - t_d)^2$$
$$+ A_{pbl1} (h - x - t_d - t_{pbl})^2 \quad (6)$$
$$+ A_{pbl2} (h - x - t_d - t_{pbl} - h_1)^2 + A_{pbl3} (h_4 - x)^2]$$
$$+ A_{pbl2} (h - x - t_d - t_{pbl} - h_1)^2 + A_{pbl3} (h_4 - x)^2]$$

(2) Case 2: $\varepsilon_0 < \varepsilon_c < \varepsilon_{cu}, x \le h_4$ and $x \le \frac{\varepsilon_{cu}}{\varepsilon_{cu} + \varepsilon_{fu}}$

As above, the resultant point of the concrete can be determined as

$$C = \int_0^x \sigma_c b da$$
$$= \int_0^{x_0} f_c \left[2\frac{\varepsilon_c}{\varepsilon_0} - \left(\frac{\varepsilon_c}{\varepsilon_0}\right)^2 \right] b da + \int_{x_0}^x f_c b da \quad (7)$$
$$= f_c x b \left(\frac{19x - h}{18x} \right)$$

The depth of the compression zone can be calculated using the equilibrium conditions, and the flexural capacity can be expressed as

$$M_u = f_c x b \left(\frac{19x - h}{18x} \right) x_c$$
$$+ \frac{E_f \varepsilon_{fu}}{h - x} [A_d (h - x - t_d)^2 \quad (8)$$
$$+ A_{pbl1} (h - x - t_d - t_{pbl})^2$$
$$+ A_{pbl2} (h - x - t_d - t_{pbl} - h_1)^2 + A_{pbl3} (h_4 - x)^2]$$

To simplify the design procedure, the ACI 440 method is applied here to go a step further. The flexural capacity of this composite deck can be calculated from Eqs. (9) and (10). In Eqs. (9) and (10), f_{yu} is determined as 0.8 times the f_u according to the test result that the ultimate tensile strain of the GFRP plate in the static test is about 0.8 times as the ultimate tensile strain of tensile samples.

$$M_u = A_d f_{yu} (d - \frac{\beta_1 c}{2}) d \quad (9)$$

$$c = \left(\frac{\varepsilon_{cu}}{\varepsilon_{cu} + \varepsilon_{fu}} \right) d \quad (10)$$

Table 4 tabulates the measured and calculated results for the proposed and ACI 440 methods, and Fig.10 shows the comparison of calculated and experimental flexural capacity. It shows that the proposed method could reasonably represent the flexural capacity, although it slightly overestimates the flexural capacity. The ACI 440 method is relatively conservative and inferior to the former method in accuracy, but it is superior in convenience. Therefore, both methods can be applied to calculate the flexural capacity of this composite deck, and a reduction coefficient should be used for safety in practical applications.

6. Analysis of shear capacity

Based on the existing experimental data, Park *et al* (2006) developed a strain-based shear strength model for members without transverse reinforcement, and it is cited and revised here to analyze the behavior of the specimens subjected to shear. Some assumptions are presented to facilitate the design procedure.

(1) The concrete in the tension zone might crack and its strength was therefore neglected.
(2) The PBL connectors were only designed to resist longitudinal shear stress, and the concrete dowels could not resist transverse shear stress.

The Rankine criterion is applied here to describe the behavior of concrete in a shear-compression zone, in which the concrete will fail if the stress exceeds the corresponding tensile strength. It can be expressed as

$$\sigma = -\frac{\sigma_u}{2} - \sqrt{(\frac{\sigma_u}{2})^2 + \upsilon_u^2} \le f_t \quad (11)$$

In Eq. (11), σ_u can be regarded as a function of the height of the natural axis, z, and the expression above can be modified as

$$\upsilon_u(z) = \sqrt{f_t [f_t + \sigma_u(z)]} \quad (12)$$

Then, the shear capacity can be determined as

$$V_c = \lambda_s b d \int_0^x \upsilon_u(z) d_z \approx \lambda_s [\sqrt{f_t (f_t + \overline{\sigma})}] x b \quad (13)$$

where

$$\overline{\sigma} = \frac{\alpha \varepsilon_0 E_c}{2} \qquad (14)$$

$$f_t = 0.395 f_{cu}^{0.55} \qquad (15)$$

$$\lambda_s = 1.2 - 0.0002a \geq 0.65 \qquad (16)$$

Eq. (13) indicates that the failure process can be divided into four stages, which can be referred to as the elastic stage, the post-crack stage, the crack propagation stage and the failure stage. Meanwhile, the shear capacity varies with the crack propagation and is minimized when the principal diagonal crack stretches to the same height as the natural axis. According to the approach of Park *et al.* (2006), the relationship between the depth of the compression zone and the compressive strain at the extreme compression fiber of the cross section can be obtained from

$$\frac{x}{d} = \frac{-E_f \varepsilon_0 \frac{A_d}{A} \alpha + \sqrt{(E_f \varepsilon_0 \frac{A_d}{A} \alpha)^2 + 4 E_f \varepsilon_0 \frac{A_d}{A} \alpha (\alpha - \frac{\alpha^2}{3}) f_c}}{2(\alpha - \frac{\alpha^2}{3}) f_c} \qquad (17)$$

$$\alpha \varepsilon_0 = \frac{2(\frac{f_{cr} h^2}{6x_0} + 0.05 \sqrt{f_c} d)(x_0 + h - x)}{E_c x (d - \frac{x}{3})} \qquad (18)$$

where

$$f_{cr} = 0.625 \sqrt{f_c} \qquad (19)$$

In Eq. (18), x_0 denotes the initial location of the principal diagonal crack, which can be determined in a simplified way (Krefeld and Thurston 1966) as

$$x_0 = 0.6a - h + x \qquad (20)$$

Finally, the shear capacity of this composite deck can be obtained by solving the resulting Eqs. (13)-(20) simultaneously. In Table 5, shear capacities predicted by the proposed method are compared with the results of the experiment, and the average value of the ratios of the test results to the capacities predicted by the proposed method is 1.06, with a coefficient of variation of 0.18. This result indicates that the proposed method can accurately predict the shear capacity of this composite deck, although it underestimates the shear capacities of the specimens that have relatively low shear span aspect ratios. This deficiency could be made up by utilizing the strut-and-tie method for those exceptional members.

A simplified method is put forward here on the basis of Chinese code (GB 50010 2010) because the design procedure mentioned above requires solving a nonlinear set of equations to obtain the final results, which is slightly complicated and tedious. The shear capacity is calculated from the following widely used equation:

$$V_c = \beta \frac{1.75}{\lambda + 1} f_t b h \qquad (21)$$

where a reduction coefficient, β, is employed here to describe the composite state of the concrete near the PBL connectors, with a value of 0.8. In Table 5, shear capacities predicted by the simplified method are compared with the results of the experiment, and the average value of the ratios of the test results to the capacities predicted by the simplified method was 1.01, with a coefficient of variation of 0.11.

Meanwhile, the results based on ACI 440 are also listed in Table 5. It should be noted that the method of ACI 440 excessively underestimates the shear capacities of the specimens. Fig. 11 shows the comparison of calculated and experimental shear capacity. These results suggest that the proposed and simplified method provide a reliable means of predicting the shear capacity of this composite deck.

7. Conclusions

This paper presented an experiment on the behavior and capacity of a GFRP-concrete composite deck, in which all of the specimens were subjected to monotonic loading conditions. Seven simply supported composite deck specimens were tested, with the shear span aspect ratio as the main parameter. The main conclusions drawn from this study are as follows:

All of the specimens failed in the anticipated pattern, namely three specimens with high shear span aspect ratios failed in typical flexural patterns, while the specimens with low shear span aspect ratios exhibited shear failure patterns.

All of the specimens demonstrated a high load-bearing capacity, while exhibiting slightly brittle behavior in the failure stage due to the linear elasticity of GFRP material. However, the development of split-tear cracks could be regarded as an effective warning of final failure.

The GFRP PBL connectors were sufficiently reliable, and there was no obvious slippage observed at the interface between the GFRP plate and the concrete, which indicated that the deck specimens were thoroughly composite.

Based on the test results, methods for predicting the flexural capacity and shear capacity of this composite deck were proposed. Meanwhile, methods proposed in ACI 440 were also applied as a comparison. By comparing the results calculated using the proposed models to the experimental results, it indicated that the proposed methods sightly overestimated both the flexural and shear capacity but still were verified to be valid. Therefore, reduction coefficients were suggested for safety in practical applications. The results based on ACI 440 methods agreed well the tested flexural capacity, but excessively underestimated the tested shear capacity.

Innovative Research Team of Xi'an University of Architecture and Technology.

References

AASHTO (2012), AASHTO LRFD Bridge Design Specifications, Washington, DC, USA.

ACI 440R (2006), Guide for the Design and Construction of Structural Concrete Reinforced with FRP Bars; MI, USA.

Cho, K., Park, S.Y., Kim, S.T. and Cho, J.R. (2010), "Shear connection system and performance evaluation of FRP-concrete composite deck", *KSCE J. Civil Eng.*, **14**(6), 855-865.

GB 50010 (2010), Code for design of concrete structures; Beijing, China. [In Chinese]

GB/T 1447 (2005), Fiber-reinforced plastics composites – Determination of tensile properties, Beijing, China. [In Chinese]

Hanus, J.P., Bank, L.C. and Oliva, M.G. (2009), "Combined loading of a bridge deck reinforced with a structural FRP stay-in-place form", *Constr. Build. Mater.*, **23**(4), 1605-1619.

He, J., Liu, Y., Chen, A. and Dai, L. (2012), "Experimental investigation of movable hybrid GFRP and concrete bridge deck", *Constr. Build. Mater.*, **26**(1), 49-64.

JTG D60 (2015), General Code for Design of Highway Bridges and Culverts; Beijing, China. [In Chinese]

Kaw, A.K. (2006), *Mechanics of Composite Materials*, CRC Press, New York, NY, USA.

Keller, T., Schaumann, E. and Vallée, T. (2007), "Flexural behavior of a hybrid FRP and lightweight concrete sandwich bridge deck", *Compos. Part A – Appl. Sci. Compos.*, **38**(3), 879-889.

Krefeld, W.J. and Thurston, C.W. (1966), "Studies of the shear and diagonal tension strength of simply supported reinforced concrete beams", *ACI Journal*, **63**(2), 451-476.

Mirmiran, A., Shahawy, M. and Beitleman, T. (2001), "Slenderness limit for hybrid GFRP-concrete columns", *J. Compos. Construct.*, **5**(1), 26-34.

Neto, A.B.D.S.S. and La Rovere, H.L. (2010), "Composite concrete/GFRP slabs for footbridge deck systems", *Compos. Struct.*, **92**(10), 2554-2564.

Pantelides, C.P., Liu, R. and Reaveley, L.D. (2012), "Lightweight concrete precast bridge deck panels reinforced with glass fiber-reinforced polymer bars", *ACI Struct. J.*, **109**(6), 879-888.

Park, H.G., Choi, K.K. and Wight, J.K. (2006), "Strain-based shear strength model for slender beams without web reinforcement", *ACI Struct. J.*, **103**(6), 783-793.

Sarir, P., Shen, S.L. and Arulrajah, A. (2016), "Concrete wedge and coarse sand coating shear connection system in GFRP concrete composite deck", *Constr. Build. Mater.*, **114**, 650-655.

Xin, H. (2015), "Thermal analysis on composite girder with hybrid GFRP-concrete deck", *Steel Compos. Struct., Int. J.*, **19**(5), 1221-1236.

Xin, H., Liu, Y. and He, J. (2015), "Fatigue behavior of hybrid GFRP-concrete bridge decks under sagging moment", *Steel Compos. Struct., Int. J.*, **18**(4), 925-946.

Zhu, J. and Lopez, M.M. (2014), "Performance of a lightweight GFRP composite bridge deck in positive and negative bending regions", *Compos. Struct.*, **113**(1), 108-117.

CC

Notation

The following symbols are used in this paper:

a = shear span;

A_d = area of GFRP plate;

A_{pbl1} = area of flange of $\perp$ shape connectors;

A_{pbl2} = area of PBL connectors under the hole;

A_{pbl3} = area of PBL connectors above the hole;

b = width of composite deck;

c = height of compression zone of concrete at balanced condition;

d = the distance from the midpoint of GFRP plate to the top of the composite deck;

E_f = modulus of elasticity of GFRP plate;

E_c = modulus of elasticity of concrete;

f_c = prism compressive strength of concrete; f_c = $0.8f_{cu}$;

f_{cu} = cubic compressive strength of concrete;

f_{cr} = cracking strength of concrete;

f_t = tensile strength of concrete;

f_{yu} = effective strength of GFRP plate;

f_u = ultimate strength of GFRP plate;

h = height of composite deck;

h_1 = height of PBL connectors below the hole;

h_2 = diameter of the hole in PBL connectors;

h_3 = height of PBL connectors above the hole;

h_4 = distance from the top of PBL connectors to the top of the composite decks;

M_u = flexural capacity;

t_d = thickness of GFRP plate;

t_{pbl} = thickness of PBL connectors;

V_u = shear capacity

x = height of compression zone of concrete;

x_0 = distance from crack point to the support;

$\alpha = \varepsilon_c/\varepsilon_0$;

β_1 = factor relating depth of equivalent rectangle compressive stress block to neutral axis;

ε_0 = peak strain of concrete subjected to compression, $\varepsilon_0 = 0.002$;

ε_{cu} = ultimate strain of concrete subjected to compression;

ε_{fu} = ultimate strain of GFRP plate;

ε_c = compressive strain at the extreme compression fiber of the cross section;

ε_f = strain of GFRP plate;

$\bar{\sigma}$ = average stress in shear-compression zone;

λ = shear span aspect ratio, $\lambda = a/h$;

λ_s = size effect factor.